Article ID: 1000-7032(2022)04-0509-09

1.5 μm Laser Properties of Large Mode Field Er^{3+}/Yb^{3+} Co-doped Microstructured Fiber Cone

WANG Ling-ling[1], XU Peng-fei[2], ZHOU De-chun[2*]

(1. *Department of Energy and Power Engineering, Shanxi Institute of Energy, Jinzhong* 030600, *China*
2. *School of Materials Science and Engineering, Changchun University of Science and Technology, Changchun* 130022, *China*)
* *Corresponding Author, E-mail: paper_paper_2017@126.com*

Abstract: The waveguide structures of large-mode-field double-cladding microstructured optical fiber and fiber cone were designed by the full vector finite element method. The microstructured optical fiber with the composition of $45Bi_2O_3$-$29GeO_2$-$15Ga_2O_3$-$10Na_2O$-$1CeO_2$ has been prepared by the cluster drawing method. Moreover, the fiber's core diameter is 70 μm, the inner cladding duty cycle is 0.25, and the mode field area is about 3 014.8 μm^2. The fiber cone with a core diameter of 17.5 μm and an effective mode field area of 206.47 μm^2 was prepared by using the fused biconical taper technology. The laser characteristics of the fiber and its cone were studied under 980 nm LD pumped. The results show that the central wavelength of the excitation spectrum of fiber drifted from 1 550.2 nm to 1 546.9 nm after tapering. And the output laser beam quality factor M^2 of fiber and fiber cone decreased significantly from 3.45 ± 0.03 to 1.16 ± 0.01. The slope efficiency of fiber and fiber cone reaches 10.29% and 9.70%, respectively. The results indicate that the taper can effectively improve the laser output mode of microstructured optical fiber, and the laser output of fiber cone has good single model characteristics. Fiber taper technology provides a new approach for preparing large-mode-field and high-power laser fiber materials.

Key words: Er^{3+}/Yb^{3+} co-doped; microstructure fiber taper; mode field; 1.5 μm laser characteristics
CLC number: TN253 **Document code**: A **DOI**: 10.37188/CJL.20220010

大模场 Er^{3+}/Yb^{3+} 共掺锥形微结构光纤 1.5 μm 激光特性

王玲玲[1], 许鹏飞[2], 周德春[2*]

(1. 山西能源学院 能源与动力工程系, 山西 晋中 030600; 2. 长春理工大学 材料科学与工程学院, 吉林 长春 130022)

摘要: 采用全矢量有限元法设计了一种大模场双包层微结构光纤及锥形波导结构。采用复丝拉制方法制备了成分为 $45Bi_2O_3$-$29GeO_2$-$15Ga_2O_3$-$10Na_2O$-$1CeO_2$ 的大模场双包层微结构光纤,纤芯直径为 70 μm,内包层的占空比为 0.25,模场面积约为 3 014.8 μm^2。采用熔融拉锥技术制备了纤芯直径为 17.5 μm、有效模场面积为 206.47 μm^2 的锥形光纤。在 980 nm 泵浦下研究了微结构光纤及其锥体的激光特性。结果表明,拉锥后微结构光纤的激发光谱中心波长由 1 550.2 nm 向短波漂移至 1 546.9 nm,而输出激光光束质量因子 M^2 由 3.45 ± 0.03显著减少至 1.16 ± 0.01。拉锥前后的斜率效率分别达到 10.29 % 和 9.70 %。研究结果表明,拉锥可有效改善大模场双包层有序微结构光纤的激光输出模式,拉锥后的激光输出具有良好的单模特性。该项技术研究结果为大模场、高功率的激光光纤材料制备提供了新的技术途径。

关 键 词: Er^{3+}/Yb^{3+} 共掺; 微结构光纤光锥; 模场; 1.5 μm 激光特性

收稿日期: 2022-01-07; **修订日期**: 2022-01-28
基金项目: 吉林省科学技术发展计划重点研发项目(20210203046SF, 20200401053GX, 20200404163YY)资助
Supported by Department of Science and Technology of Jilin Province(20210203046SF, 20200401053GX, 20200404163YY)

1 Introduction

The near-infrared 1.5 μm laser has become a research hotspot owing to the wide range of applications in many fields such as biomedicine, environmental detection, space communications, infrared countermeasures, and guidance[1-4]. Er^{3+} single-doped or Er^{3+}/Yb^{3+} co-doped microstructured optical fiber(hereinafter referred to as MOF) is an important way to generate high-power laser output in the 1.5 μm band[5-6]. This paper uses bismuth germanate glass as the host glass to prepare rare-earth-doped optical fiber. Bismuth germanate glass is expected to combine the advantages of bismuth glass and germanate glass, such as lower phonon energy, high refractive index, wider infrared transmission range, and good rare-earth ion solubility, which provides low laser pumping threshold and high pump absorption efficient. Compared with traditional optical fibers, MOF can achieve large-mode-field area, high-power single-mode laser output by effectively controlling the duty cycle and core[7-8]. Meanwhile, MOF has the advantages of a large numerical aperture and high coupling efficiency[9-11]. Fiber cone is drawn based on fiber through secondary processing technology. Its internal microstructure and cone shape make it have a large-mode-field area, adjustable dispersion, high nonlinear effect, non-cut-off single model, low transmission loss, and good beam quality[12-18]. Fiber cone has new applications in many fields. In 2017, Petersen *et al.* demonstrated the ability of tapered large-mode-area $Ge_{10}As_{22}Se_{68}$ PCFs to generate broadband MIR SC with record high output power above 4.5 μm[19]. In 2018, Mao *et al.* realized all-fiber flexible cylindrical vector lasers at 1 550 nm using fiber cones[20]. Previous studies have shown that the nonlinear effect of optical fiber can be reduced by shortening the length of optical fiber and increasing the core diameter[21-22]. However, with the increase in core diameter, the fiber laser no longer works in the single-mode state, and the quality of the output laser beam becomes poor. As the power continues to rise, there will be some scientific issues such as nonlinear effects, heat dissipation, laser damage, *etc*[23-26]. The design of a large-mode-field double-cladding Er^{3+}/Yb^{3+} co-doped MOF cone can avoid these problems and is an effective way to increase the output power further[27-30]. The excellent characteristics of rare earth doped MOF provide a new technical approach for high-power and high brightness fiber lasers.

In this paper, a waveguide structure of large-mode-field double-cladding MOF was designed based on Er^{3+}/Yb^{3+} co-doped $45Bi_2O_3$-$29GeO_2$-$15Ga_2O_3$-$10Na_2O$-$1CeO_2$ (hereinafter referred to as BGGN) glass. The full vector finite element method and the numerical analysis methods were used to study the optimal structural parameters of the MOF during single-mode operation. Furthermore, the main structural parameters such as the lattice constant (hole spacing) and the duty cycle of the MOF were determined. The large-mode-field Er^{3+}/Yb^{3+} co-doped MOF and its cone were prepared using the cluster drawing method and the fused biconical taper technology. The spectral and laser characteristics were studied. Finally, a self-designed linear cavity-structured fiber laser achieved a single-mode laser output of 1 546.9 nm in the fiber cone, and its beam quality factor M^2 reached 1.16 ± 0.01.

2 Experiments

2.1 Structural Design of MOF and Analytical Method

The MOF is an optical waveguide with triangular air pores in the cladding in this study. The guided mode propagates in the lattice defects in a process analogous to total internal reflection, that is, the flaws create the MOF core. Fig. 1 shows the cross-section of bismuthate glass microstructure fiber. The number of microporous lattice layers in the inner cladding is 5, the core diameter is 70 μm, and the outside cladding is 488 μm. Before and after taper drawing, the fiber cone keeps the effective duty ratio at 0.25, the inner cladding air hole diameter at 10 μm, and the lattice constant at 40 μm.

The full vector finite element method(FEM) uses matrix analysis to solve related algebraic equations.

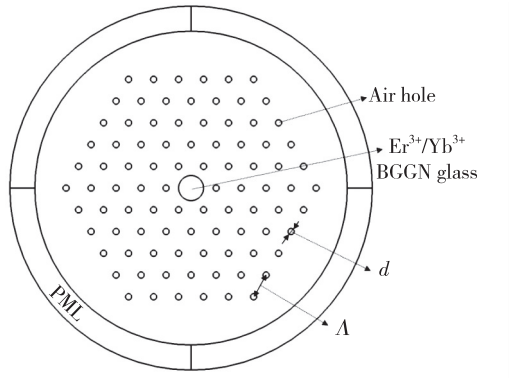

Fig. 1　Cross-section of bismuthate glass microstructure fiber

The discrete Maxwell equation is used to express the fluctuation of each cell in the transverse diffusion section of the optical fiber. The waveguide equation is solved for an approximate solution in the full fiber mode field[31]. For example, the two sides of a MOF cladding cell are ideal magnetic conductors(Fig. 2). The fundamental mode $HE_{11}^{\ y}$ polarized in the y-direction and $HE_{11}^{\ x}$ of the fundamental mode polarized in the x-direction. The effective refractive index of the fundamental space-filling mode can be calculated by using complete vector finite element analysis (Fundamental space-filling mode, FSM).

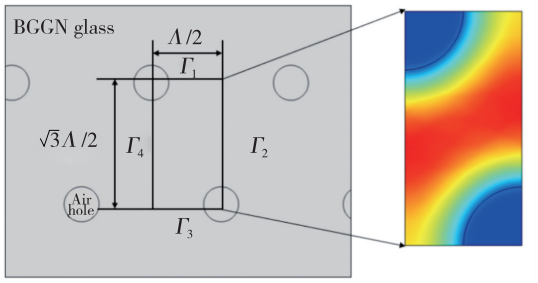

Fig. 2　The cell calculation unit of MOF cladding

The wave optics model of the MOF is developed through using FEM in this study, and the theoretical simulation calculation of the wave optics model of the MOF is performed using the absorption boundary condition of the perfectly matched layer.

As with regular step-index fibers, Birks and Knight *et al.* reported in 1997[32] that the comparable normalized frequency V_{eff} is:

$$V_{\text{eff}} = \frac{2\pi}{\lambda} R_{\text{eff}} \sqrt{n_{\text{core}}^2 - n_{\text{FSM}}^2}, \tag{1}$$

where n_{core} is the refractive index of the core material at the MOF's working wavelength, n_{FSM} is the effective refractive index of the FSM, and R_{eff} is the MOF's equivalent core radius. The single-mode operation can be maintained when V_{eff} is less than 2.405.

For triangular microstructure fiber, Park *et al.* gave a functional relationship of equivalent core radius based on hole spacing and duty cycle in 2005[33]:

$$\frac{R_{\text{eff}}}{\Lambda} = \frac{c_1}{1 + \exp[(d/\Lambda - c_3)/c_2]}, \tag{2}$$

the values of c_1, c_2 and c_3 in the formula are 0.686 064, 0.265 366 and 1.291 080, respectively. Based on the fundamental mode effective refractive index n_{eff} and the cladding effective refractive index n_{FSM}, the theoretical numerical aperture (NA) of the inner cladding can be computed:

$$\text{NA} = (n_{\text{eff}}^2 - n_{\text{FSM}}^2)^{1/2}. \tag{3}$$

The following equation can be used to calculate the effective mode field area of the MOF[34]:

$$A_{\text{eff}} = \frac{(\iint |E(x,y)|^2 \mathrm{d}x\mathrm{d}y)^2}{\iint |E(x,y)|^4 \mathrm{d}x\mathrm{d}y}, \tag{4}$$

where A_{eff} is the effective mode field area of the MOF, $E(x,y)$ is the electric field distribution of the cross section of the fiber, and the integral region is the section of the whole fiber.

2.2　Sample Preparation

The cladding glass is composed of $45Bi_2O_3$-$29GeO_2$-$15Ga_2O_3$-$10Na_2O$-$1CeO_2$. The core glass samples with molar compositions of $45Bi_2O_3$-$29GeO_2$-$15Ga_2O_3$-$10Na_2O$-$1CeO_2$-$0.5Er_2O_3$-xYb_2O_3 (where x = 0, 1, 2, 2.5, named as B_1 to B_4) were prepared by melt-quenching method. The sample was weighed accurately and melted in an alumina oxide crucible at 1 200 ℃ for about 50 min under a dry O_2/N_2 atmosphere to reduce the OH^- content. Then it was quenched in preheated stainless steel blocks and annealed at the glass transition temperature for 3 h. Finally, the annealed glass sample was cut and polished to the size of 10 mm × 10 mm × 2 mm with two parallel sides for optical and spectroscopic measurements.

The core glass rod was prepared by the melt-quenching method, and was drawn into a core rod with a diameter of 4.2 mm and a cutting length of 280 mm by a fiber drawing machine. The bundled

drawing method was used to draw it into an Er^{3+}/Yb^{3+} co-doped MOF with a diameter of 488 μm, the core diameter was 70 μm, the inner cladding air hole diameter d was 10 μm, the lattice constant Λ is 40 μm, and the duty ratio $d/\Lambda = 0.25$. The MOF was drawn into a fiber cone with a diameter of 122 μm, a core diameter of 17.5 μm, a length of the taper region of 30 mm, and a taper angle of 0.7° using the fused biconical taper technology.

2.3 Measurements

The absorption spectra were measured with a Perkin Elmer Lambda 950-type spectrophotometer. The measurement of infrared fluorescence spectrometry employs the Horiba Jobin Yvon's Fluorolog-3 fluorescence spectrometer. In addition, the output quality of the fiber laser before and after the taper was measured by knife-edge method. AQ6370D spectrum analyzer manufactured by Yokogawa was used to detect the optical signal. The output power at the output end of the optical fiber was recorded by using a Newport 2936-R optical power meter. All the tests were performed at room temperature.

3 Results and Discussion

3.1 Spectral Analysis of Er^{3+}/Yb^{3+} Co-doped BGGN Core Glass

The absorption spectra of $B_1 - B_4$ glass are shown in Fig. 3. The absorption peaks at 1 530, 980, 800, 650, 543, 520, 487 nm correspond to the Er^{3+} ion from the ground state $^4I_{15/2}$ to the excited state $^4I_{13/2}$, $^4I_{11/2}$, $^4I_{9/2}$, $^4F_{9/2}$, $^4S_{3/2}$, $^2H_{11/2}$ and $^4F_{7/2}$, respectively. Obviously, the absorption peak near 980 nm is very strong which is caused by the spectral overlap of Yb^{3+} ion energy level $^2F_{7/2} \rightarrow {}^2F_{5/2}$ and the Er^{3+} ion energy level $^4I_{15/2} \rightarrow {}^4I_{11/2}$. Therefore, the pump efficiency of 980 nm LD can be improved by the energy transfer between the energy level $^2F_{5/2}$ of Yb^{3+} and the energy level $^4I_{11/2}$ of Er^{3+}. Owing to the absorption cross section of Yb^{3+} being larger than that of Er^{3+}, and the concentration of Yb^{3+} is several times that of Er^{3+}, the absorption peak increases with the increase of Yb^{3+} ion concentration.

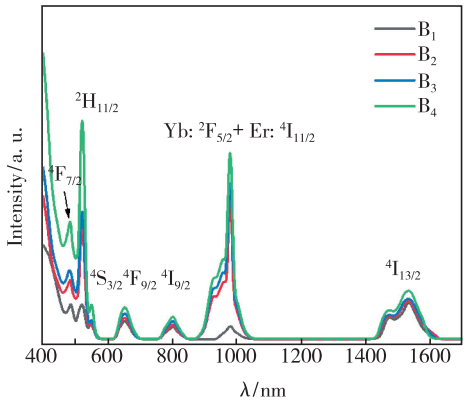

Fig. 3 Absorption spectra of BGGN glass samples

Fig. 4 shows the 1.53 μm fluorescence spectra in Er^{3+}/Yb^{3+} co-doped BGGN glass. It can be seen from the figure that the fluorescence intensity of about 1.53 μm is significantly enhanced after Yb^{3+} ions are doped. The highest emission intensity around 1.5 μm is achieved at around 2% Yb_2O_3 concentration. This is because the sensitization of Yb^{3+} ions improves the pump efficiency of 980 nm LD. However, due to the concentration quenching effect and anti-cross relaxation effect of Yb^{3+} ions, when the doping concentration of Yb^{3+} ions reach 2.5% or more, the energy cannot be effectively forwarded Er^{3+} ions, which makes the 1.53 μm fluorescence intensity in the B_4 glass decrease significantly. Hence, the optimum doping ratio of Er^{3+}: Yb^{3+} is 0.5%:2%.

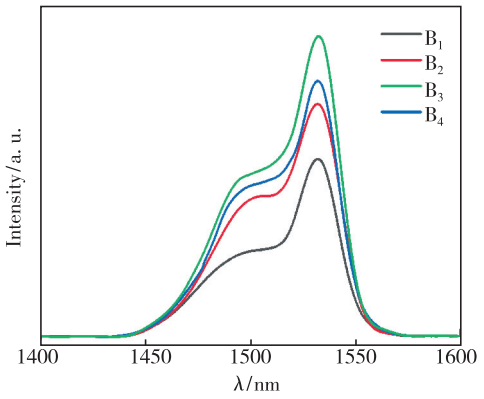

Fig. 4 Fluorescence spectra of the BGGN glass samples

3.2 Cut-off Characteristic Analysis

The finite element method was used to study the relationship between different duty cycles and the normalized final frequency of the fiber. In this paper, the lattice constant Λ of inner cladding layer

is 10 – 60 μm(Λ is 10, 20, 30, 40, 50, 60 μm in order, and the working wavelength is 1.55 μm). According to formula (1), under different conditions of d/Λ, the relationship curve between the V_{eff} and d/Λ was obtained in Fig. 5. It can be seen that, with $d/\Lambda = 0.25$ and $\Lambda = 10$, the V_{eff} of MOF is less than 2.405, and the laser can achieve single-mode operation. At this time, the air hole diameter d of the inner cladding capillary glass should be 2.5 μm, and the duty cycle should be 0.25.

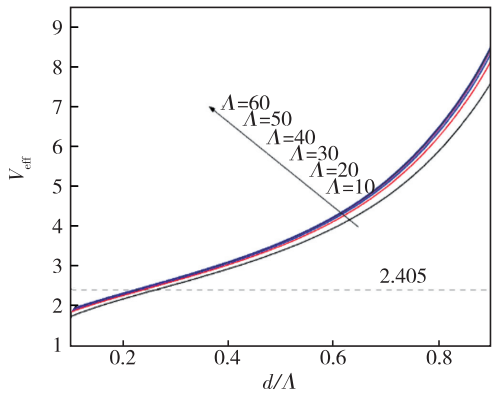

Fig. 5　Relationship between normalized cut-off frequency V_{eff} and inner cladding duty cycle

3.3　Mode Field and Numerical Aperture

The structural parameters of fiber and fiber cone were verified and calculated by using the full vector finite element method. Fig. 6 shows the structure and mode-field energy distribution. It should be emphasized that the optical field of this MOF is approximately hexagonal, and the core has the strongest optical field. The mode field diameters and effective mode field areas of fiber and fiber cone are 65.661 μm, 3 014.8 μm^2, 17.603 μm and 206.47 μm^2, respectively. The results show the parameters of the fiber cone can meet the single-mode operation of large-mode-field lasers[35-36].

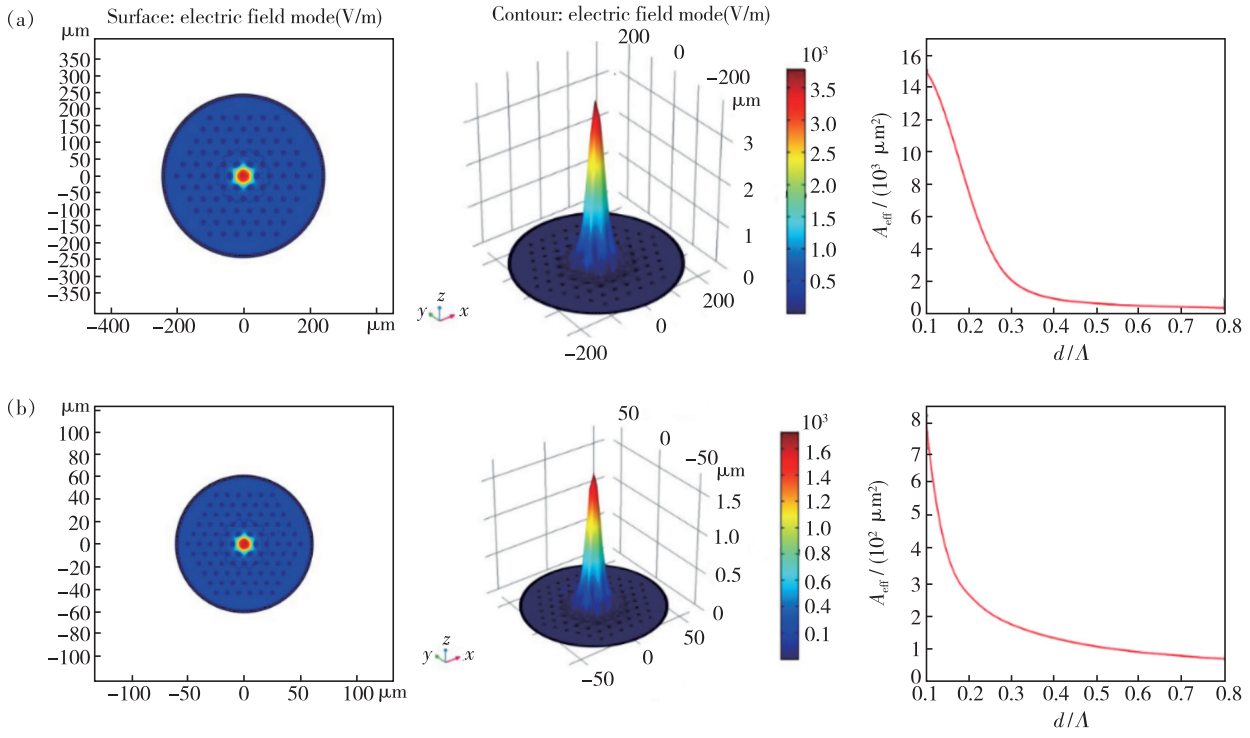

Fig. 6　Structure and mode field energy distribution with effective duty ratio $d/\Lambda = 0.25$. (a) Fiber. (b) Fiber cone.

The inner cladding numerical aperture (NA) represents the ability of optical fiber collecting incident pump light, which is directly related to the coupling efficiency of the pump light[37]. Therefore, increasing the NA is important for improving the coupling efficiency of pump light. In this paper, the outer cladding air holes were selected as the cell calculation unit, the hole spacing P and the diameter D of the outer cladding air holes were used as the key variables. When the hole spacing P is 1, 2, 3, 4, 5 μm in order, the relationship curve between the NA of the inner cladding and the duty cycle D/P of the

outer cladding is shown in Fig. 7. Obviously, the NA increases with the D/P increasing. Under the same duty cycle condition, the smaller P is, the larger NA is. When P is less than 2 μm, the theoretical maximum value of NA can reach above 0.8. Therefore, this work determine the hole spacing P after taper is 2 mm, D/P is 0.98, and D is 1.96 mm.

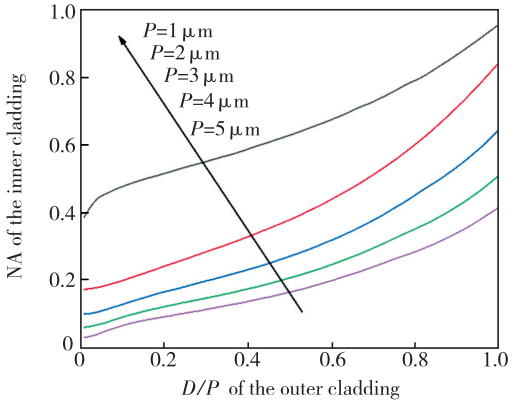

Fig. 7 The relationship curve between NA and D/P

At the same time, the optimal NA of the inner cladding could reach 0.75, which is larger than the tapered MOF (0.6) reported by Duan in 2020[38].

3.4 Laser Characteristics Analysis

Fig. 8 is the schematic diagram of a laser measuring apparatus for Er^{3+}/Yb^{3+} co-doped BGGN MOF. The laser uses 980 nm LD as the pump source and a self-made Er^{3+}/Yb^{3+} co-doped BGGN fiber with a length of 30 cm as the gain medium. Fig. 9 is a cross section microscopic image of self-made optical fiber. The pump source pigtail is coupled into the inner cladding of the double-clad Er^{3+}/Yb^{3+} co-doped fiber through a collimating lens and a focusing lens. The laser cavity consists of a front cavity mirror which is a dichroic mirror(980 nm high transmission 98%, 1 530 nm high reflection greater than 99%) closing to the input end of the fiber, and a rear cavity mirror which is Fresnel reflection putting at the output end of the fiber.

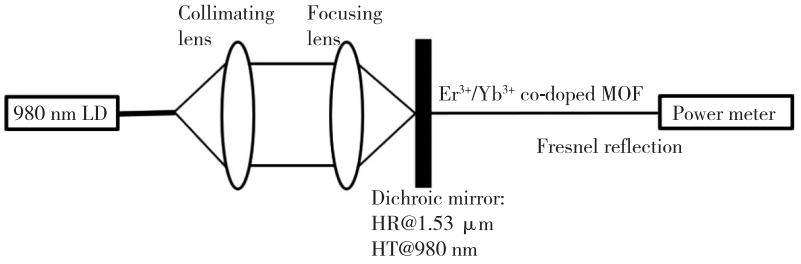

Fig. 8 Structure of Er^{3+}/Yb^{3+} co-doped microstructure fiber laser

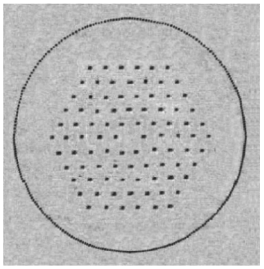

Fig. 9 MOF cross section microscopic image

Fig. 10 shows the laser output spectrum of the fiber and fiber cone. The center wavelength of the excitation spectrum of the MOF laser is 1 550.2 nm and 1 546.9 nm, respectively. The taper causes the excitation center wavelength of the laser shifting to short waves. The reason for this phenomenon is that the lasing wavelength of a fiber laser is related to the fiber length and the excitation threshold. The fiber length has less change after tapering, but the intracavity loss of the excitation light in the fiber core increases, which increases the laser's excitation threshold. Meanwhile, an increase in the excitation threshold corresponds to a short wavelength lasing wavelength. Therefore, the fiber taper technology moves the laser's lasing wavelength toward the short-wave direction.

The Er^{3+}/Yb^{3+} co-doped MOF and its cone with a length of 30 cm were pumped with 980 nm LD. Fig. 11 is the relationship curve between output power and pump power. The laser output of fiber can be observed when the pumping power of the fiber is 239 mW. When the pumping power reaches 581 mW, the maximum laser output power is 55.7 mW. According to the measured data, a linear fit was performed in the above threshold range, and the

slope efficiency of the fiber was 10.29%. The maximum output power of fiber cone under the same conditions is 50.12 mW, the slope efficiency is 9.70%, and the maximum output power is reduced by about 10%. This is because after taper drawing, the hole spacing becomes smaller, and the confinement loss of all modes increases. The disappearance of high-order modes and the rise in the confinement loss of the base mode are the main reasons for reducing laser output power.

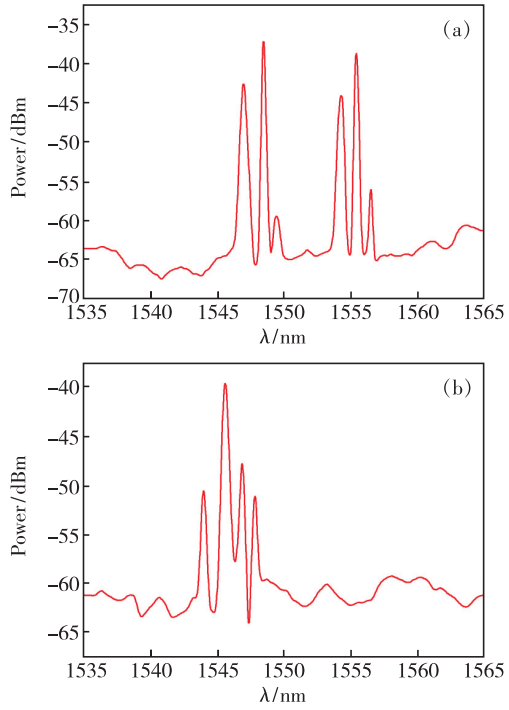

Fig. 10　Laser spectra of fiber(a) and fiber cone(b)

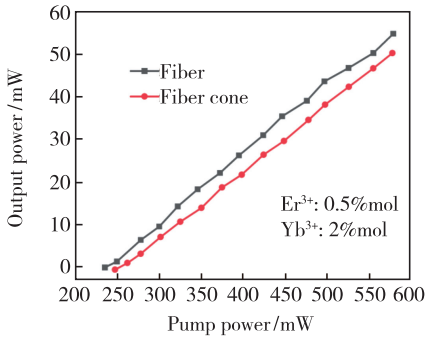

Fig. 11　Laser output power characteristic curve of fiber and fiber cone

At the output end of the Er^{3+}/Yb^{3+} co-doped MOF, the knife-edge method was used to measure the laser output beam quality of fiber and fiber cone. The results are shown in Fig. 12. The quality factor M^2 of the fiber and fiber cone is 3.45 ± 0.03 and 1.16 ± 0.01. Taper makes the output beam quality factor M^2 of the laser smaller than before, and the laser output has a good single-mode.

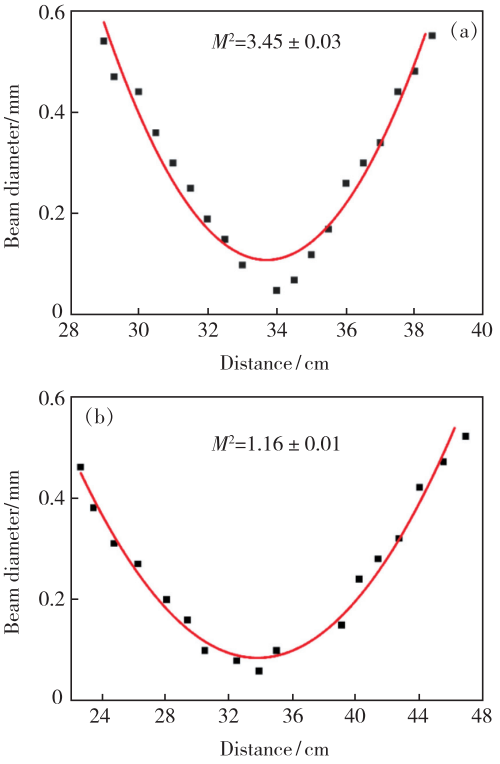

Fig. 12　Laser output beam quality M^2 of fiber(a) and fiber cone(b)

4　Conclusion

The waveguide structures of a large-mode-field double-cladding MOF and its cone were designed by the full vector finite element method. The Er^{3+}/Yb^{3+} co-doped optical fiber and fiber cone with composition $45Bi_2O_3$-$29GeO_2$-$15Ga_2O_3$-$10Na_2O$-$1CeO_2$ were prepared by using the cluster drawing method and the fused biconical taper technology. The core diameters of fiber and its cone were 70 μm and 17.5 μm. The mode field areas were about 3 014.8 μm^2 and 206.47 μm^2, the inner cladding duty cycle d/Λ of fiber and fiber cone were both 0.25. The optimal numerical aperture of the inner cladding of the MOF cone is 0.75, which can significantly improve the coupling efficiency of the pump light. The laser characteristics of fiber and its cone were studied under 980 nm LD. Results show that the taper makes the center wavelength of the excitation spectrum of the MOF laser drift from 1 550.2 nm to 1 546.9

nm. The slope efficiency of fiber and fiber cone can reach 10.29% and 9.70%, respectively. The output laser beam quality factor M^2 is significantly reduced from 3.45 ± 0.03 to 1.16 ± 0.01. This research provides a new approach for preparing large-mode-field, high-power laser fiber materials.

Response Letter is available for this paper at: http://cjl.lightpublishing.cn/thesisDetails#10.37188/CJL.20220010.

References:

[1] DOBLER J T, HARRISON F W, BROWELL E V, *et al.* Atmospheric CO_2 column measurements with an airborne intensity-modulated continuous wave 1.57 μm fiber laser lidar [J]. *Appl. Opt.*, 2013, 52(12): 2874-2892.

[2] LADACI A, GIRARD S, MESCIA L, *et al.* Radiation hardened high-power Er^{3+}/Yb^{3+}-codoped fiber amplifiers for free-space optical communications [J]. *Opt. Lett.*, 2018, 43(13): 3049-3052.

[3] CHEN Y J, LIN Y F, YANG Z M, *et al.* Eye-safe 1.55 μm Er∶Yb∶$YAl_3(BO_3)_4$ microchip laser [J]. *OSA Continuum.*, 2018, 2(1): 142-150.

[4] ZHOU D C, JIN D Y, LAN Z D, *et al.* Preparation of Er^{3+}/Yb^{3+} co-doped citrate microstructure fiber of large mode field and its 3.0 μm laser performance [J]. *J. Am. Ceram. Soc.*, 2019, 102(4): 1686-1693.

[5] ZHANG J, FROMZEL V, DUBINSKII M. Resonantly cladding-pumped Yb-free Er-doped LMA fiber laser with record high power and efficiency [J]. *Opt. Express*, 2011, 19(6): 5574-5578.

[6] CHEN Z M, TU X, ZHAO J J, *et al.* An erbium-doped fiber whispering-gallery-mode microcavity laser [J]. *IEEE. Photonic Technol. Lett.*, 2019, 31(20): 1650-1653.

[7] WANG W, XU H D, YANG Q H, *et al.* Large mode area microstructured fiber supporting 56 super-OAM modes [J]. *Opt. Express*, 2019, 27(20): 27991-28008.

[8] PRUDENZANO F, MESCIA L, ALLEGRETTI L, *et al.* Simulation of mid-IR amplification in Er^{3+}-doped chalcogenide microstructured optical fiber [J]. *Opt. Mater.*, 2009, 31(9): 1292-1295.

[9] ZHU Z M, BROWN T G. Full-vectorial finite-difference analysis of microstructured optical fibers [J]. *Opt. Express*, 2002, 10(17): 853-864.

[10] FRANCO M A R, SERRAO V A, SIRCILLI F. Microstructured optical fiber for residual dispersion compensation over $S+C+L+U$ wavelength bands [J]. *IEEE Photonic Technol. Lett.*, 2008, 20(9): 751-753.

[11] TOWN G E, YUAN W, MCCOSKER R, *et al.* Microstructured optical fiber refractive index sensor [J]. *Opt. Lett.*, 2010, 35(6): 856-858.

[12] MÄGI E C, STEINVURZEL P, EGGLETON B J. Tapered photonic crystal fibers [J]. *Opt. Express*, 2004, 12(5): 776-784.

[13] LIMPERT J, SCHMIDT O, ROTHHARDT J, *et al.* Extended single-mode photonic crystal fiber lasers [J]. *Opt. Express*, 2006, 14(7): 2715-2720.

[14] SCHMIDT O, ROTHHARDT J, EIDAM T, *et al.* Single-polarization ultra-large-mode-area Yb-doped photonic crystal fiber [J]. *Opt. Express*, 2008, 16(6): 3918-3923.

[15] KUMAR A, SAINI T S, NAIK K D, *et al.* Large-mode-area single-polarization single-mode photonic crystal fiber: design and analysis [J]. *Appl. Opt.*, 2016, 55(19): 4995-5000.

[16] LI L, SCHÜLZGEN A, TEMYANKO V L, *et al.* Short-length microstructured phosphate glass fiber lasers with large mode areas [J]. *Opt. Lett.*, 2005, 30(10): 1141-1143.

[17] SAGHAEI H. Dispersion-engineered microstructured optical fiber for mid-infrared supercontinuum generation [J]. *Appl. Opt.*, 2018, 57(20): 5591-5598.

[18] FUJIWARA M, TOUBARU K, NODA T, *et al.* Highly efficient coupling of photons from nanoemitters into single-mode optical fibers [J]. *Nano Lett.*, 2011, 11(10): 4362-4365.

[19] PETERSEN C R, ENGELSHOLM R D, MARKOS C, *et al.* Increased mid-infrared supercontinuum bandwidth and average power by tapering large-mode-area chalcogenide photonic crystal fibers [J]. *Opt. Express*, 2017, 25(13): 15336-15348.

[20] MAO D, HE Z W, LU H, *et al.* All-fiber radially/azimuthally polarized lasers based on mode coupling of tapered fibers

[J]. *Opt. Lett.*, 2018,43(7):1590-1593.

[21] BAKER C C,FRIEBELE E J,BURDETT A A,*et al.* Nanoparticle doping for high power fiber lasers at eye-safer wavelengths [J]. *Opt. Express*, 2017,25(12):13903-13915.

[22] EIDAM T,WIRTH C,JAUREGUI C,*et al.* Experimental observations of the threshold-like onset of mode instabilities in high power fiber amplifiers [J]. *Opt. Express*, 2011,19(14):13218-13224.

[23] ZERVAS M N,CODEMARD C A. High power fiber lasers:a review [J]. *IEEE J. Sel. Top. Quantum Electron.*, 2014, 20(5):219-241.

[24] PENG K,ZHAN H,NI L,*et al.* Single-mode large-mode-area laser fiber with ultralow numerical aperture and high beam quality [J]. *Appl. Opt.*, 2016,55(35):10133-10137.

[25] JAUREGUI C,LIMPERT J,TÜNNERMANN A. High-power fibre lasers [J]. *Nat. Photonics*, 2013,7(11):861-867.

[26] RICHARDSON D J,NILSSON J,CLARKSON W A. High power fiber lasers:current status and future perspectives [Invited] [J]. *J. Opt. Soc. Am.* B, 2010,27(11):B63-B92.

[27] SONG X Y,JIN D Y,ZHOU D C,*et al.* Er^{3+}/Yb^{3+} co-doped bismuthate glass and its large-mode-area double-cladding fiber for 1.53 μm laser [J]. *J. Alloys Compd.*, 2021,853:157305.

[28] SLIMEN F B,CHEN S X,LOUSTEAU J,*et al.* Highly efficient-Tm^{3+} doped germanate large mode area single mode fiber laser [J]. *Opt. Mater. Express*, 2019,9(10):4115-4125.

[29] ROBIN C A,HARTL I,ROY V,*et al.* Yb-doped large mode area tapered fiber with depressed cladding and dopant confinement [C]. *Proceedings of SPIE* 10083, *Fiber Lasers* XIV: *Technology and Systems*, *San Francisco*, *United States*, 2017:1008314-1-6.

[30] LIMPERT J,STUTZKI F,JANSEN F,*et al.* Yb-doped large-pitch fibres:effective single-mode operation based on higher-order mode delocalisation [J]. *Light Sci. Appl.*, 2012,1(4):e8-1-5.

[31] KOSHIBA M. Full-vector analysis of photonic crystal fibers using the finite element method [J]. *IEICE. Trans. Electronics*, 2002,E85-C(4):881-888.

[32] BIRKS T A,KNIGHT J C,RUSSELL P S J. Endlessly single-mode photonic crystal fiber [J]. *Opt. Lett.*, 1997,22(13): 961-963.

[33] PARK K N,LEE K S. Improved effective-index method for analysis of photonic crystal fibers [J]. *Opt. Lett.*, 2005,30 (9):958-960.

[34] MATSUI T,SAKAMOTO T,TSUJIKAWA K,*et al.* Single-mode photonic crystal fiber design with ultralarge effective area and low bending loss for ultrahigh-speed WDM transmission [J]. *J. Lightwave Technol.*, 2011,29(4):511-515.

[35] SAITOH K,TSUCHIDA Y,KOSHIBA M,*et al.* Endlessly single-mode holey fibers:the influence of core design [J]. *Opt. Express*, 2005,13(26):10833-10839.

[36] MORTENSEN N A. Effective area of photonic crystal fibers [J]. *Opt. Express*, 2002,10(7):341-348.

[37] ISSA N A. High numerical aperture in multimode microstructured optical fibers [J]. *Appl. Opt.*, 2004,43(33): 6191-6197.

[38] DUAN D W,KAVATAMANE V K,ARUMUGAM S R,*et al.* Tapered ultra-high numerical aperture optical fiber tip for nitrogen vacancy ensembles based endoscope in a fluidic environment [J]. *Appl. Phys. Lett.*, 2020,116(11):113701-1-5.

王玲玲(1966 –),女,山西兴县人,博士,正高级工程师,2017 年于长春理工大学获得博士学位,主要从事大口径光纤锥及光纤传像器件的机理、制备及性能的研究。
E-mail: ccoewll@163.com

周德春(1964 –),男,吉林长春人,博士,教授,博士生导师,2011 年于长春理工大学获得博士学位,主要从事光纤材料与器件的机理、制备、激光性能及应用的研究。
E-mail: paper_paper_2017@126.com